Supplementary Information

Bimetal CoNi-Metal-Organic Frameworks@molybdenum disulfide Core-shell Z-Scheme Heterojunctions with Broad-Spectrum Response Toward Optimized Photocatalytic Performance

Xinyue Liu[a], Zipeng Xing[a,*], Na Zhang[a], Tao Cheng[a], Bo Ren[a], Weizi Chen[a], Zibin Wang[a], Zhenzi Li[b,*], Wei Zhou[b,*]

[a] *Heilongjiang Provincial Key Laboratory of Environmental Nanotechnology, School of Chemistry and Materials Science, Heilongjiang University, Harbin 150080, P. R. China.,*

Tel: +86-451-8660-8616, Fax: +86-451-8660-8240,

Email: xingzipeng@hlju.edu.cn

[b] *Shandong Provincial Key Laboratory of Molecular Engineering, School of Chemistry and Chemical Engineering, Qilu University of Technology (Shandong Academy of Sciences), Jinan, Shandong, 250353, P. R. China*

Email: zzli@qlu.edu.cn; zwchem@hotmail.com

Experimental section

Materials

Cobalt chloride hexahydrate ($CoCl_2 \cdot 6H_2O$) and nickel chloride hexahydrate ($NiCl_2 \cdot 6H_2O$) were purchased from Tianjin Kemer Chemical Reagent Co., LTD. The phthalic acid (BDC), ammonium molybdate ($(NH_4)_2MoO_4$), and thiouroid (CH_4N_2S) were purchased from Aladdin BioTechnologies Inc. N, N-dimethylformamide (DMF) and ethanol (ET) were purchased from Shanghai Maclin Biochemical Technology Co., LTD.

Characterizations

The powder X-ray diffraction (XRD) patterns were acquired on a Bruker D8 Advance diffractometer by using Cu Kα radiation (λ = 1.5406 Å). Scanning electron micros-copy (SEM) images were obtained with a Philips XL-30-ESEM-FEG instrument operating at 20 kV. Transmission electron microscope (TEM) JEOL JEM-2010 at an accelerating voltage of 200 kV was also used to record the electron micrographs of the samples. X-ray photoelectron spectroscopy (XPS) was measured on a PHI-5700 ESCA instrument with Al-Kα X-ray source. UV-vis diffuse reflection spectra (DRS) were recorded on a UV-vis spectrophotometer (UV-2550, Shimadzu) with an integrating sphere attachment, and $BaSO_4$ was used as the reference material. Fourier transform infrared spectra (FT-IR) were detected with a PerkinElmer spectrum one system. The N_2 adsorption-desorption isotherms at 77 K were collected on an AUTOSORB-1 (Quantachrome Instruments) nitrogen adsorption apparatus. Surface area was estimated by BET method and pore-size distribution was measured

from the adsorption branch of the isotherm using the Barrett-Joyner-Halenda (BJH) method. The steady-state photoluminescence (PL) spectra were measured with a PE LS 55 spectrofluoro-photometer at excitation wavelength of 325 nm. Scanning Kelvin probe (SKP) measurements (SKP5050 system, Scotland) were performed at normal laboratory conditions. The electron spin resonance (ESR) spectra under visible light irradiation were tested with ESR spectrometer (Bruker model A300). The temperature of the sample was measured using the Testo 865 infrared thermograph.

Photocatalytic degradation

In order to test the photocatalytic ability under visible light irradiation (light source is 300 W Xenon lamp), we degrade Persistent Organic Dyes Rhodamine B at room temperature (20 ± 2 ^{o}C). In a typical experiment, 30 mg of photocatalyst and 15 mg of PMS was added to a Rhodamine B solution (30 mL, 10 mg L^{-1}), and then the suspension was placed in the dark for 30 min to ensure adsorption equilibrium. The suspension was irradiated with a 300 W Xenon lamp equipped with a filter ($\lambda \geq 420$ nm). The residual concentration of Rhodamine B was analyzed by a T6 UV-Vis spectrophotometer.

Photocatalytic hydrogen evolution

The photocatalytic hydrogen evolution was tested in an online photocatalytic hydrogen evolution system (Au Light, Beijing, CEL-SPH2N) at room temperature. In a typical process, 50 mg of photocatalysts were suspended in 100 mL aqueous closed gas circulation reaction cell which include 80 mL deionized water and 20 mL of methanol used as the sacrificial reagent. Afterward, the suspension was purged with

N_2 for several times to remove O_2 and CO_2. After that, the suspension solution was irradiated by a 300 W Xeon-lamp equipped with an AM 1.5 G filter (Oriel, USA), and use an on-line gas chromatography (SP7800, TCD, molecular sieve 5 Å, N_2 carrier, Beijing Keruida, Ltd) to analyze the hydrogen periodically with the interval of every 1h.

Photoelectrochemical measurements

Photoelectrochemical measurements of photocatalysts were detected in a three-electrode system with the CHI760E electrochemical workstation. The electrolyte selected KOH solution (1 M), the reference electrode selected Ag/AgCl and the opposite electrode selected Pt. Then, 0.1 g of photocatalysts were mixed with 3 mL of ethanol at stirring for 10 min, and sprayed on the FTO-glass of 1 × 2 cm^2 further heating and drying. The photocurrent tests were extra monitored under AM 1.5G light exposure.

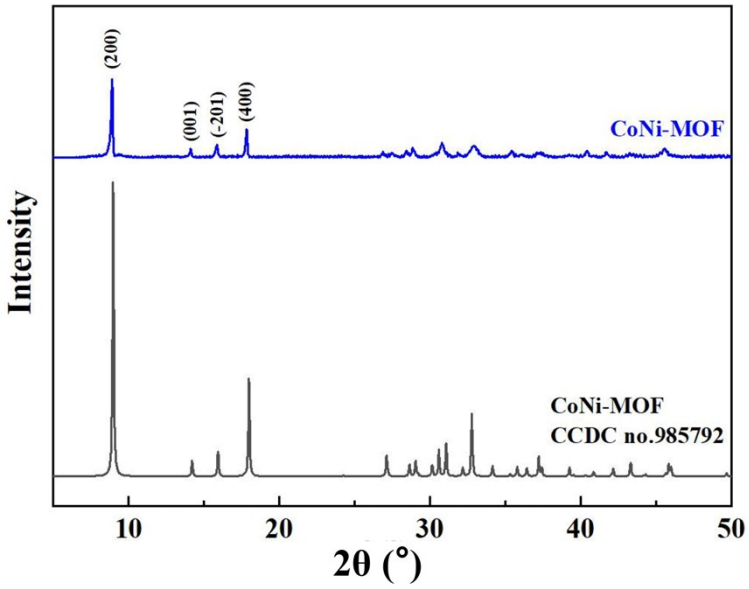

Fig. S1 The XRD pattern of CoNi-MOF.

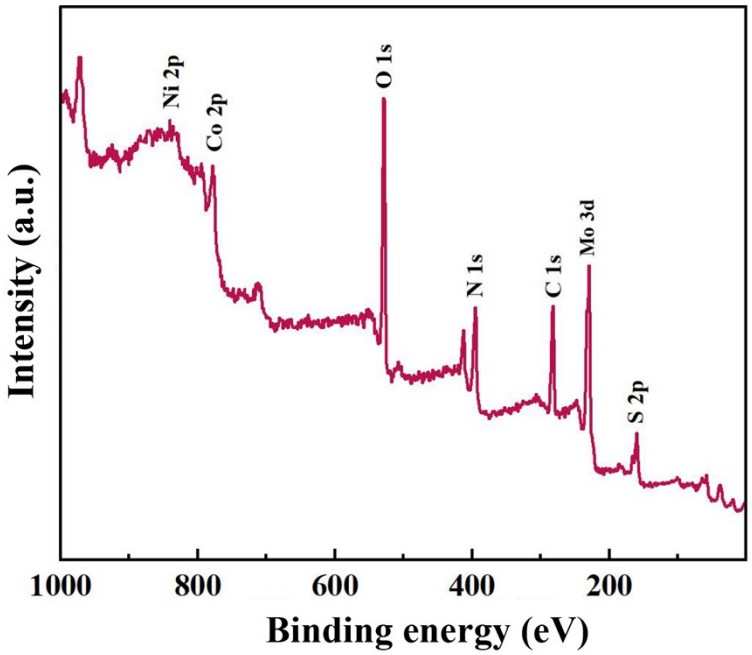

Fig. S2 The XPS full scan of CoNi-MOF@MoS_2.

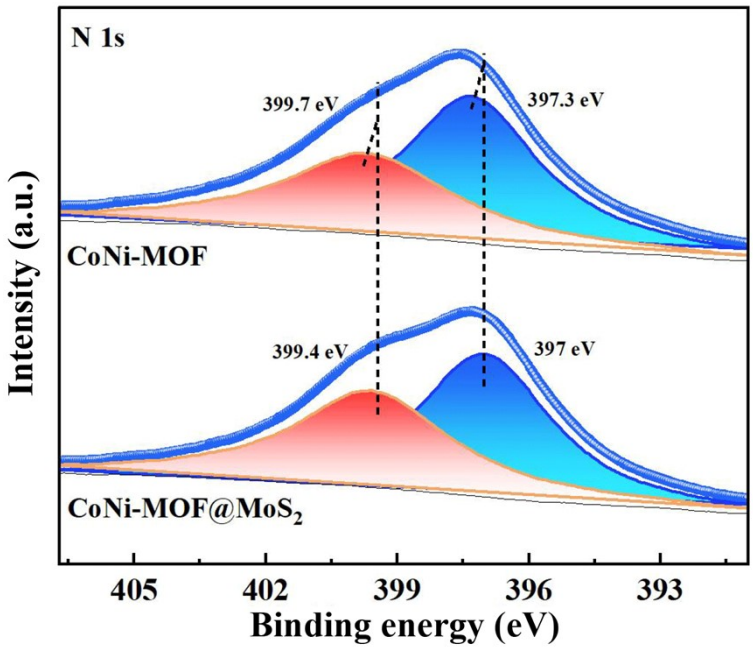

Fig. S3 The XPS spectra of N 1s for CoNi-MOF and CoNi-MOF@MoS_2, respectively.

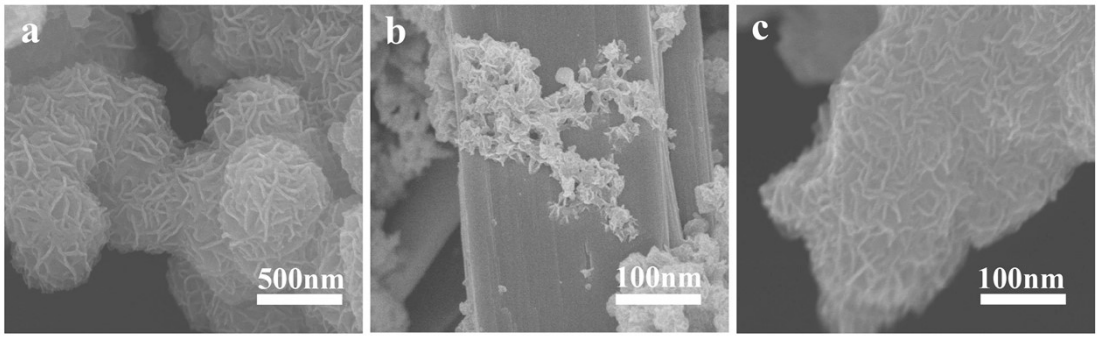

Fig. S4 SEM images of MoS_2 (a), CoNi-MOF@MoS_2-0.075 (b), CoNi-MOF@MoS_2-0.12 (c).

.

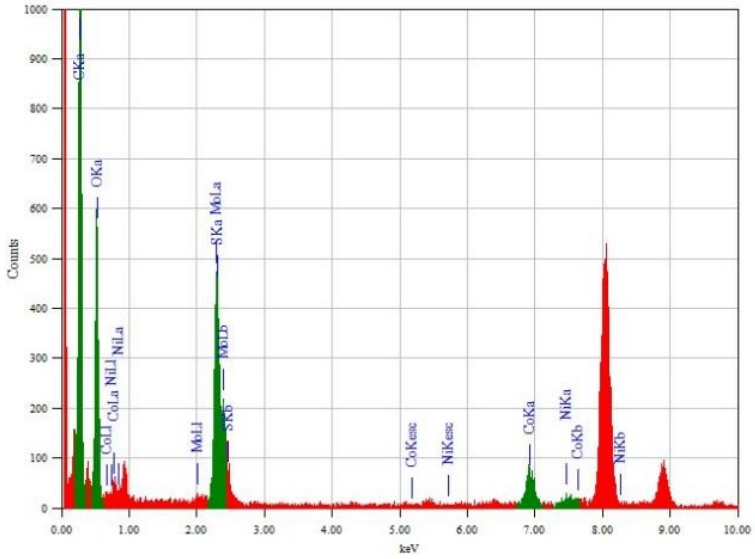

Fig. S5 EDX elemental spectrum of CoNi-MOF@MoS_2.

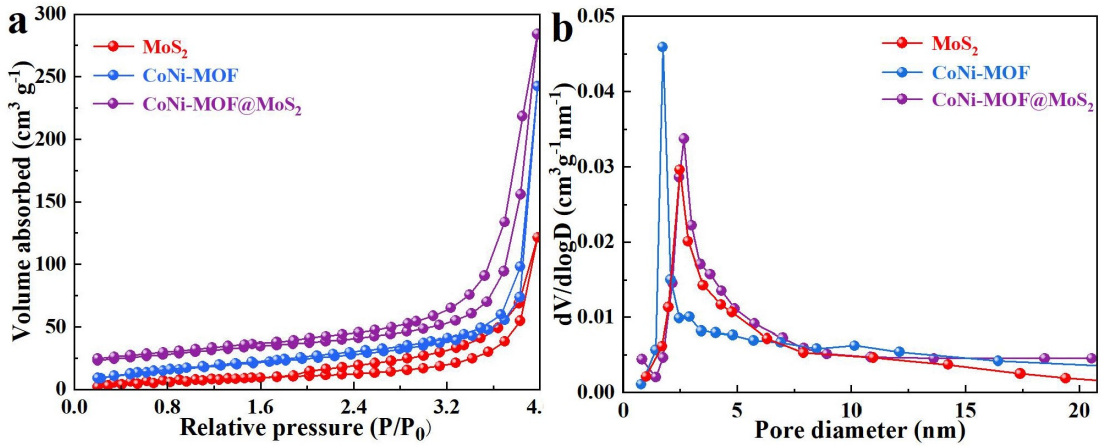

Fig. S6 N_2 adsorption-desorption isotherms for CoNi-MOF, MoS_2, and CoNi-MOF@MoS_2 (a) and the corresponding BJH pore size distributions (b).

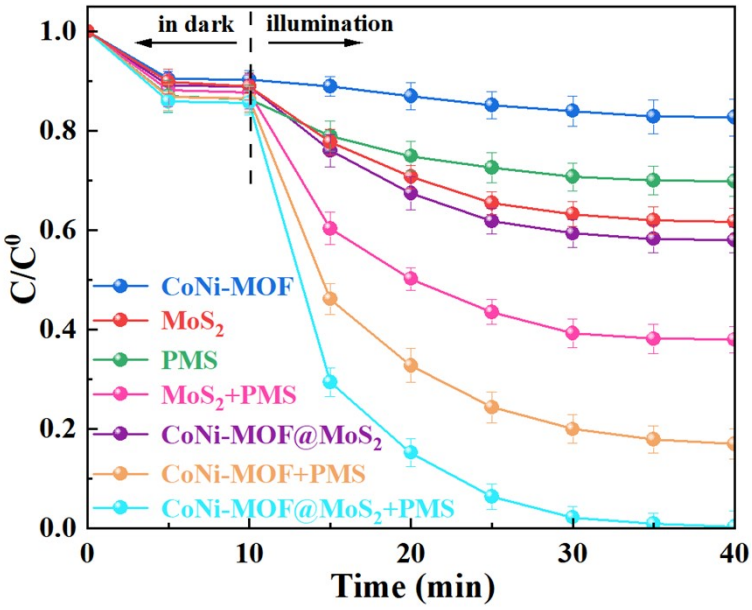

Fig. S7 The photocatalytic degradation of MO by MoS_2, CoNi-MOF, PMS, CoNi-MOF@MoS_2 with PMS.

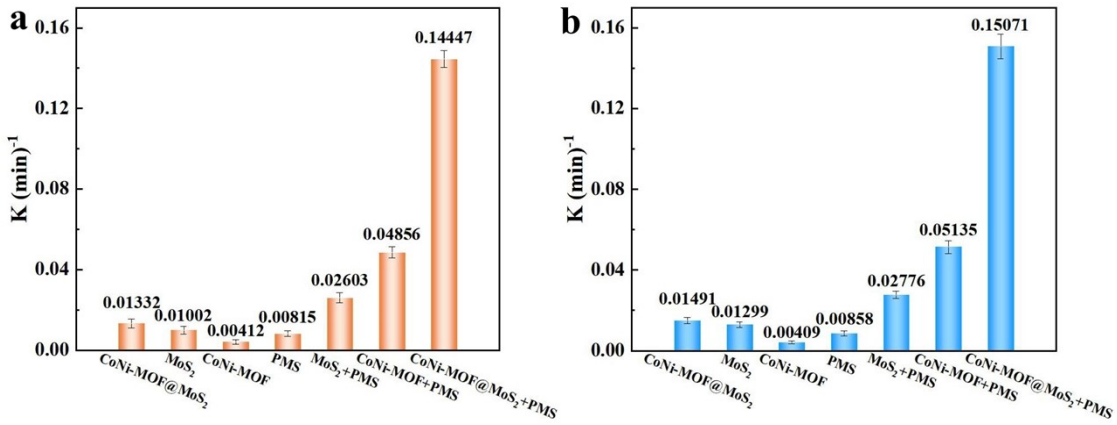

Fig. S8 First order reaction rate constants (K) of RhB and MO photocatalytic degradation.

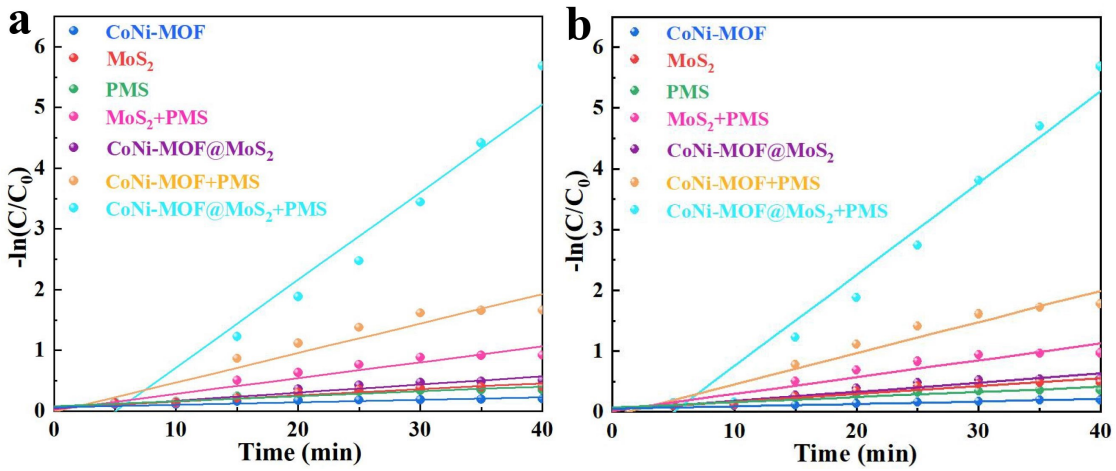

Fig. S9 First order kinetic curves of RhB (a) and MO (b) degradation by different photocatalysts.

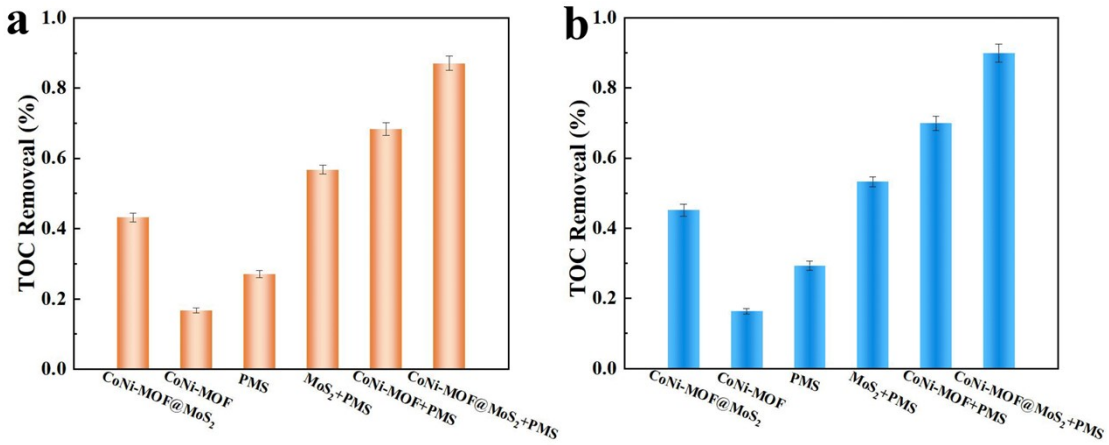

Fig. S10 TOC removal efficiency of as-prepared samples for the degradation of RhB (a) and MO (b) for different samples.

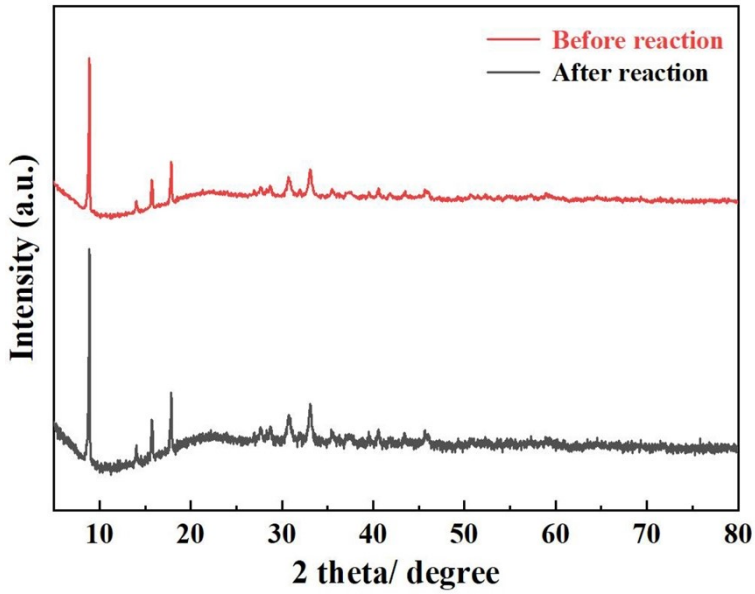

Fig. S11 The XRD patterns of CoNi-MOF@MoS_2 before and after photocatalytic reaction, respectively.

.

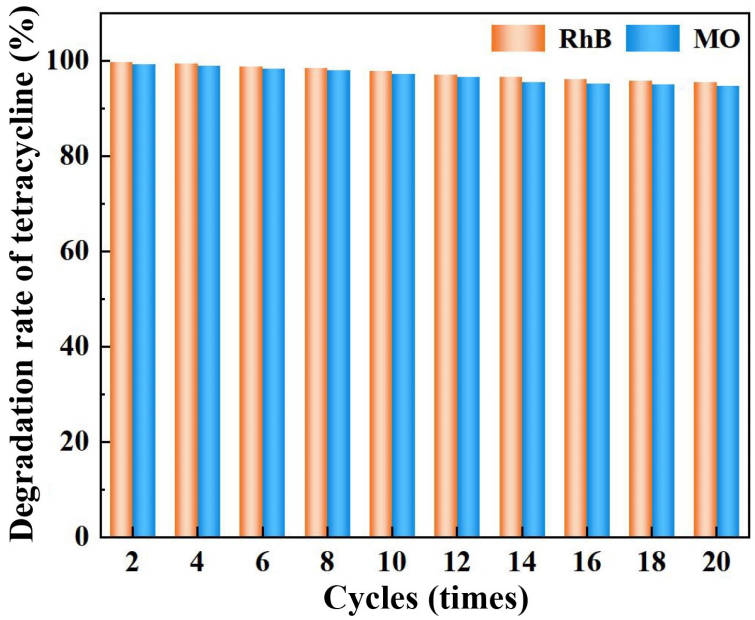

Fig. S12 Long-term stability cycling tests of photocatalytic degradation RhB and MO by CoNi-MOF@MoS_2.

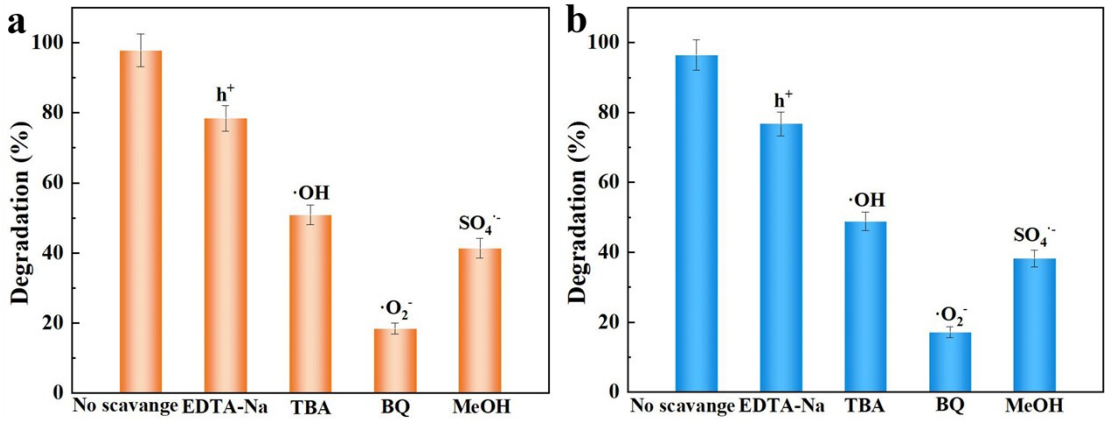

Fig. S13 Trapping experiments of RhB (a) and MO (b) degradation by CoNi-MOF@MoS_2 + PMS photocatalyst.

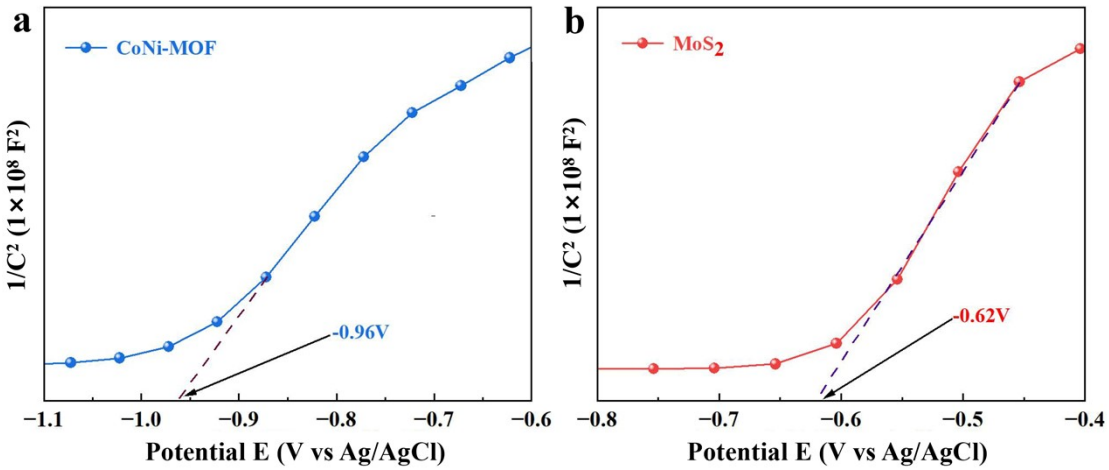

Fig. S14 Mott-Schottky plots of CoNi-MOF (a) and MoS_2 (b).

Table. S1 Comparison of photocatalytic H_2 evolution rates between CoNi-MOF@MoS_2 and other different photocatalysts under visible light irradiation.

Photocatalysts	Light source	H_2 evolution rate	Ref.
Co_3O_4/$NaTaO_3$	300 W Xe lamp (λ>420 nm)	8.05 μmol h^{-1} g^{-1}	[1]
Co-MOF/p-g-C_3N_4	300 W Xe lamp (λ>420 nm)	73.42 μmol h^{-1} g^{-1}	[2]
CPPB QDs/Ni-MOF	300 W Xe lamp (λ>420 nm)	153.6 μmol h^{-1}	[3]
C-MoS_2/g-C_3N_4	300 W Xe lamp (λ>400 nm)	157.14 μmol h^{-1} g^{-1}	[4]
MoS_2/g-C_3N_4	300 W Xe lamp (λ>420 nm)	280 μmol h^{-1} g^{-1}	[5]
CoNi-MOF@MoS_2	**300 W Xe lamp (λ>420 nm)**	**478.6 μmol h^{-1} g^{-1}**	**This work**

Table S2. Comparison toward degradation of refractory organic pollutants by with various photocatalysts.

Photocatalysts	Pollutant	Degradation time (min)	Degradation rate (%)	Ref.
g-C_3N_4/Ag/ZnO	RhB	210	70	[6]
$AgInS_2$/CN/PAN	RhB	60	94.48	[7]
ZrU@IL-1/PAN NFs	RhB	40	67	[8]
Fe-g-C_3N_4	RhB	45	95.5	[9]
BC/2ZIS/WO_3	MB	60	80.5	[10]
CoNi-MOF@MoS_2	**Organic dye**	**40**	**99.3**	**This work**

Table S3. The band gap energies (E_g), conduction band (CB) and valence band (VB) potentials (NHE) for CoNi-MOF and MoS_2.

Samples	E_g (eV)	CB (V)	VB (V)
CoNi-MOF	2.33	-0.76	1.57
MoS_2	2.2	-0.42	1.78

References

[1] D. Xu, L. Li, H. Xu, J. Zhu, W. Fan, J. Ding, W. Shi, In-situ synthesis of $Co_3O_4/NaTaO_3$ composites by electrostatic attraction from Co-MOF for water splitting, J. Solid State Chem., 280 (2019) 120986.

[2] S. Zhao, J. Xu, M. Mao, L. Li, X. Li, Protonated g-C_3N_4 cooperated with Co-MOF doped with Sm to construct 2D/2D heterojunction for integrated dye-sensitized photocatalytic H_2 evolution, J. Colloid Interface Sci., 583 (2021) 435-447.

[3] X. Zhang, M. He, H. Fang, J. Bao, X. Bu, C. Yang, X. Sheng, B. Wu, Z. Zhang, Y. Zhou, Additional electron transfer channels of thermostable 0D Cs(Pb: Pt)Br_3 perovskite quantum dots /2D accordion-like Ni-MOF nanojunction for photocatalytic H_2 evolution, Int. J. Hydrogen Energy, 47 (2022) 40860-40871.

[4] X. Wei, X. Zhang, S. Ali, J. Wang, Y. Zhou, H. Chen, G. Zhang, J. Qi, D. He, Carbon intercalated MoS_2 cocatalyst on g-C_3N_4 photo-absorber for enhanced photocatalytic H_2 evolution under the simulated solar light, Int. J. Hydrogen Energy, 48 (2023) 13827-13842.

[5] Y. Liu, X. Xu, H. Li, Z. Si, X. Wu, R. Ran, D. Weng, A Facile One Step Synthesis of MoS_2/g-C_3N_4 Photocatalyst with Enhanced Visible Light Photocatalytic Hydrogen Production, Catal. Lett., 152 (2022) 972-979.

[6] P.P. Gotipamul, G. Vattikondala, K.D. Rajan, S. Khanna, M. Rathinam, S. Chidambaram, Impact of piezoelectric effect on the heterogeneous visible photocatalysis of g-C_3N_4/Ag/ZnO tricomponent, Chemosphere, 287 (2022) 132298.

[7] X. Liang, J. Liu, H. Guo, H. Li, E. Liu, Y. Zhao, Y. Ji, J. Fan, Preparation of a recyclable and high-performance photocatalyst $AgInS_2$/CN/PAN for RhB and phenol degradation, J. Environ. Chem. Eng., 11 (2023) 109987.

[8] S. Asgari, G. Mohammadi Ziarani, A. Badiei, Y. Vasseghian, Zr-UiO-66, ionic liquid (HMIM+TFSI−), and electrospun nanofibers (polyacrylonitrile): All in one as a piezo-photocatalyst for degradation of organic dye, Chem. Eng. J., 487 (2024) 150600.

[9] S. Ji, Y. Yang, Z. Zhou, X. Li, Y. Liu, Photocatalysis-Fenton of Fe-doped g-C_3N_4 catalyst and its excellent degradation performance towards RhB, J. Water Process. Eng., 40 (2021) 101804.

[10] L. Cheng, Y. Zhang, W. Fan, Y. Ji, Synergistic adsorption-photocatalysis for dyes removal by a novel biochar–based Z-scheme heterojunction BC/2ZIS/WO_3: Mechanistic investigation and degradation pathways, Chem. Eng. J., 445 (2022) 136677.